

RESEARCH ARTICLE

10.1029/2020JD033955

Key Points:

- Stratospheric intrusion is an important factor to the enhancement of ozone (O_3) in the lower troposphere observed over Hong Kong during springtime
- Occurrence of stratospheric intrusion in the subtropical region is attributed to the large-scale subsidence associated with the upper-level subtropical jet
- The impact of stratospheric intrusion can be extended to the atmospheric boundary layer, which may lead to the increase of surface O_3

Supporting Information:

Supporting Information may be found in the online version of this article.

Correspondence to:

J. Huang,
hjpfwj@gmail.com

Citation:

Zhao, K., Huang, J., Wu, Y., Yuan, Z., Wang, Y., Li, Y., et al. (2021). Impact of stratospheric intrusions on ozone enhancement in the lower troposphere and implication to air quality in Hong Kong and other South China regions. *Journal of Geophysical Research: Atmospheres*, 126, e2020JD033955. <https://doi.org/10.1029/2020JD033955>

Received 30 SEP 2020
Accepted 23 AUG 2021

Author Contributions:

Data curation: Kaihui Zhao, Xiaodan Ma

Formal analysis: Jianping Huang, Wei Ma

Funding acquisition: Yongwei Wang

Investigation: Kaihui Zhao, Jianping Huang

Methodology: Kaihui Zhao, Yonghua Wu, Zibing Yuan, Yongwei Wang, Ying Wang

Resources: Jianping Huang, Xiaodan Ma

Software: Kaihui Zhao, Yonghua Wu, Zibing Yuan, Yongwei Wang, Xuehui Liu, Wei Ma, Ying Wang

© 2021. American Geophysical Union.
All Rights Reserved.

Impact of Stratospheric Intrusions on Ozone Enhancement in the Lower Troposphere and Implication to Air Quality in Hong Kong and Other South China Regions

Kaihui Zhao¹, Jianping Huang^{2,3,4} , Yonghua Wu⁵ , Zibing Yuan¹, Yongwei Wang⁶, Ying Li⁷ , Xiaodan Ma², Xuehui Liu¹, Wei Ma¹, Ying Wang⁸, and Xiaoyan Zhang² 

¹School of Environment and Energy, South China University of Technology, Guangzhou, China, ²Yale-NUIST Center on Atmospheric Environment, Nanjing University of Information Science & Technology, Nanjing, China, ³I.M. System Group, Environmental Modeling Center, NOAA National Centers for Environmental Prediction, College Park, MD, USA, ⁴Center for Spatial Information Science and Systems, College of Science, George Mason University, Fairfax, VA, USA, ⁵The City College of New York and NOAA-CREST, New York, NY, USA, ⁶Climate, Environment and Sustainability Center, Nanjing University of Information Science and Technology, Nanjing, China, ⁷Southern University of Science and Technology, ShenZhen, China, ⁸Xianyang Meteorological Bureau, Xianyang, China

Abstract Stratospheric intrusions are an important source of ozone (O_3) in the troposphere. In this study, 17 years of O_3 sounding data from the Hong Kong Observatory with a weekly sampling frequency are analyzed to identify stratospheric intrusions and quantify their impact on O_3 enhancement events in springtime from 2004 to 2020. 24.7% of O_3 enhancement events are related to stratospheric intrusion whereas 31.7% of intrusions lead to the enhancement of O_3 in the lower troposphere. Occurrences of stratospheric intrusion in springtime are closely related to tropopause folding and tropospheric convective activities in subtropical regions. The Weather Research and Forecasting model coupled with Chemistry simulations are conducted with the integrated process analysis to quantify the impact of stratospheric intrusions on the enhancement of O_3 in the lower free troposphere as well as near the surface under different synoptic patterns. Synoptic patterns associated with stratospheric intrusion-driving O_3 enhancements are classified into two categories: Saddle Point (“S”) and Cold Front (“F”). While downward transport of O_3 -enriched air from the enhancement layer exerts an important impact on surface O_3 for synoptic pattern “S,” the impact on surface O_3 is limited for surface pattern “F.” The impact of stratospheric intrusions together with entrainment on surface O_3 may have a strong indication on the development of effective emission control strategies on surface O_3 reduction in Hong Kong.

1. Introduction

Tropospheric ozone (O_3) is of great concern due to its importance to atmospheric chemistry, air quality, and climate change (e.g., Westervelt et al., 2019; Zhang et al., 2016). Elevated levels of ambient O_3 near the surface are harmful to human health, crop yields, and natural ecosystems (e.g., Mills et al., 2018; Monks et al., 2015; Tai et al., 2014). Tropospheric O_3 acts as an effective greenhouse gas and an important source of hydroxyl (OH) radicals, the first oxidant or “detergent of the atmosphere.” While the abundance is much less than that in the stratosphere (10% vs. 90%), tropospheric O_3 shows great variations in time and space. The large temporal and spatial variations are mainly attributed to a variety of factors such as photochemical reactions, transport, diffusion, and stratospheric intrusion (e.g., Liu et al., 2009, 2013). Given the complexity of the governing processes, it is critical to quantify their relative roles in determining O_3 variations in the troposphere.

Photochemical reactions and horizontal transport are the two important factors contributing to O_3 enhancement in the troposphere. Their roles have been widely investigated through observational and modeling studies (e.g., Lin et al., 2012; Ma et al., 2021; Verstraeten et al., 2015; Zhao et al., 2019). According to the previous studies, photochemical productions were a major factor that contributed to the increase in tropospheric O_3 since preindustrial times (e.g., Rowlinson et al., 2020; Sicard et al., 2018) and the key factor leading to O_3 exceedance events under favorable meteorological conditions on a local or regional scale

Writing – original draft: Kaihui Zhao
Writing – review & editing: Kaihui Zhao, Jianping Huang, Yonghua Wu, Zibing Yuan

(e.g., Wang et al., 2009; Zhao et al., 2019). Meanwhile, horizontal transports on regional, long-range, and intercontinental scales may convey O₃ and its precursors from polluted regions to their downstream areas, elevating the ambient levels substantially. For instance, the transport from East Asia may enhance springtime O₃ in the free troposphere over the western United States (Cooper et al., 2010; Verstraeten et al., 2015). The injection of O₃ precursor species, such as nitrogen oxides (NO_x), volatile organic compounds (VOCs), and carbon monoxide (CO), emitted from biomass burning are transported up to the free troposphere and can increase O₃ concentrations over Southeast Asia (Jian & Fu, 2014). Several large field campaigns showed that intercontinental transport from North America and Asia was an important source contributing to the increase of O₃ in remote locations such as Strath Vaich, Scotland in Europe (Fowler et al., 2001; Singh et al., 2006; Y. Tang et al., 2003).

Stratospheric intrusions are another important source of tropospheric O₃. Stratospheric intrusion is characterized by elevated O₃ concentrations (e.g., >80 ppbv), high values of potential vorticity (PV) (e.g., 1–4 PV), low relative humidity (RH) (e.g., less than 20%) from tropopause to middle troposphere (e.g., James et al., 2003; Kim & Lee, 2010), and high wind speed (e.g., >20 m/s) in the upper troposphere (Antonescu et al., 2013; Van Haver et al., 1996). Stratospheric intrusions may transport O₃-enriched air from the stratosphere downward to the troposphere and exert an important impact on temporal-spatial variations in tropospheric O₃ (Ni et al., 2019; Oltmans et al., 2004). Stratospheric intrusions or stratosphere-troposphere exchanges accounted for a change of 0.78% yr⁻¹ of tropospheric O₃ in China and 0.84% yr⁻¹ in western United States (Verstraeten et al., 2015). A modeling study showed that the global annual stratospheric intrusion O₃ flux increased by 53% from 2000 to 2100 under the Representative Concentration Pathway 8.5 Scenario that may lead to an increase in tropospheric O₃ by 3% in the northern hemisphere and 4% in the southern hemisphere (Meul et al., 2018). Meanwhile, the occurrences of stratospheric intrusion events are highly associated with the upper-level jet and the seasonal difference in intrusions is observed between low and middle latitudes where the upper-level jets are more active (e.g., Ding & Wang, 2006; Ni et al., 2019).

Entrainment may further transport O₃-enriched air from the free troposphere downward into the atmospheric boundary layer (ABL), leading to the substantial enhancement of surface O₃ (Ganguly, 2012; Langford et al., 2012; Pendlebury et al., 2018). Such an enhancement of surface O₃ is closely associated with synoptic patterns. For instance, an O₃ exceedance event occurred after a cold front passed over the western United States, while a deep stratospheric intrusion was observed (Langford et al., 2012). A strong downward transport of O₃ from the upper troposphere to near surface layer in East Asia was influenced by a moving low-pressure system (Carmichael et al., 1998). Deep convection (e.g., tropical and extratropical cyclones), a commonly recognized mesoscale process and sometimes embedded within a synoptic scale event was favorable for both stratospheric intrusion and entrainment (e.g., Akritidis et al., 2016; Frey et al., 2015; Jaeglé et al., 2017; Ni et al., 2019). Hence, synoptic patterns are a prerequisite to transport tropospheric O₃ downward into the ABL. So far, a combined impact of stratospheric intrusion with entrainment on surface O₃ is not well investigated under different synoptic patterns in Hong Kong.

Hong Kong is located at the subtropical regions where weather is influenced significantly by the East Asian Monsoon. Zhang et al. (2013) illustrated that Hong Kong was usually located in the western edge of the subtropical high over the northwestern Pacific, which was dominated by humid weather. Low-pressure systems associated with a trough are another dominant weather pattern in Hong Kong during springtime, which is accompanied by relatively low wind speed and high temperature. Unusually high O₃ concentrations (i.e., greater than 70.0 ppbv) are often observed in the lower free troposphere (i.e., about 2–4 km above ground level, AGL) during springtime (Oltmans et al., 2004; Zhao et al., 2021). Long-range transport bringing O₃-enriched air and its precursors (NO_x, VOCs, CO) from Southeast Asia to Hong Kong were a key factor accounting for O₃ enhancement in the lower troposphere during springtime (C. Y. Chan & Chan, 2000; L. Y. Chan et al., 2000; Han et al., 2019; Jian & Fu, 2014). Biomass burning, originated from the Indochina Peninsula, had an important impact on tropospheric O₃ over Southeast Chinese regions, especially during El Niño events (K. L. Chan, 2017; Lee & Cheng, 2011). O₃ sounding data indicated that O₃ enhancement along west Pacific coastal regions north of about 30°N was closely associated with the stratospheric intrusions (Oltmans et al., 2004). As a comparison, the impact of stratospheric intrusions on enhancement springtime O₃ in the lower free troposphere in the subtropical regions like Hong Kong needs to be addressed carefully (Barrett et al., 2019; Zhao et al., 2021).

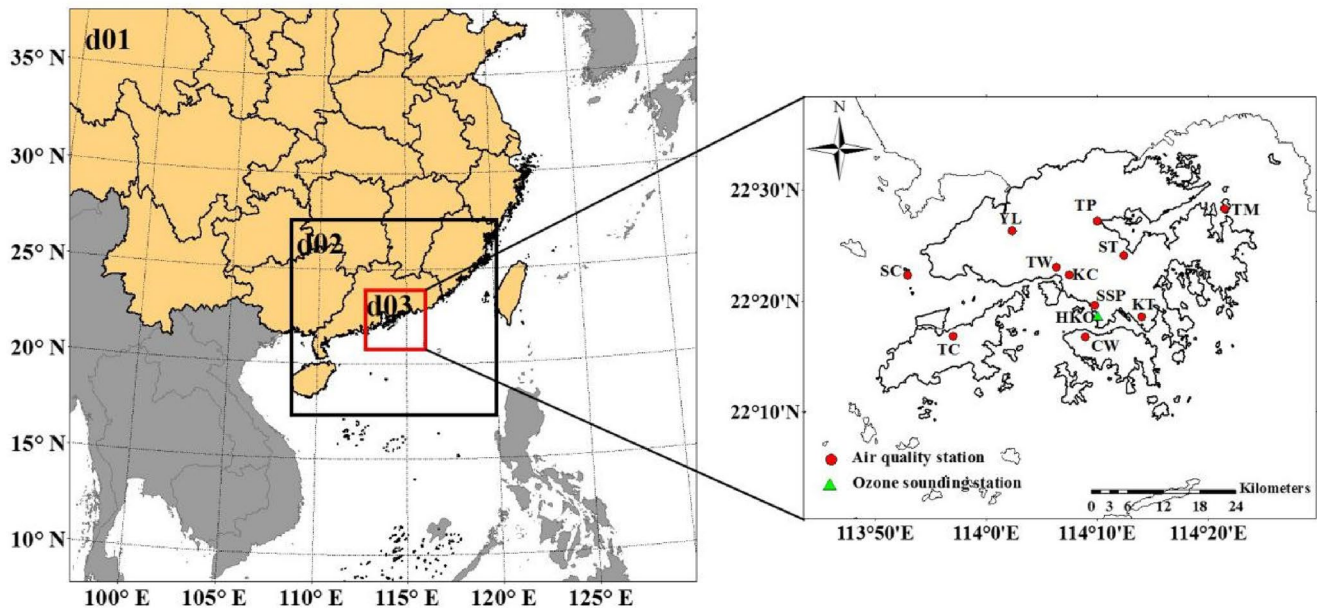


Figure 1. (a) Settings of three domains used in Weather Research and Forecasting/Chemistry simulations and (b) location of observational sites operated by the Hong Kong Environmental Protection Department (Sha Chau [SC], Yuen Long [YL], Taipo [TP], Tsuen Wan [TW], Sha Tin [ST], Tap Mun [TM], Kwai Chung [KC], Shan Shui Po [SSP], Kwun Tong [KT], Tung Chung [TC], Central Western [CW], and Hong Kong Observatory [HKO]).

In our previous study (Zhao et al., 2021), the Weather Research and Forecasting/Chemistry (WRF/Chem) model with an upper-boundary scheme demonstrated its capability in simulating stratospheric intrusion processes, but it was limited to a single case. The results did not provide sufficient evidence in support of the development of effective emission control strategies (Zhao et al., 2021). In this study, seventeen-year O_3 sounding data operated once per week by the Hong Kong Observatory (HKO, 22.31°N, 114.17°E, 66 m above sea level) are analyzed to identify stratospheric intrusion-associated O_3 enhancement events in the lower free troposphere in spring from 2004 to 2020. We present a factor analysis on the occurrence of the stratospheric intrusions in springtime over the subtropical region like Hong Kong. Synoptic patterns are then classified by an examination of the weather maps associated with stratospheric intrusion-driven enhancement of O_3 in the lower troposphere. WRF/Chem model is applied with integrated process analysis (IPR) to quantify the impacts of stratospheric intrusions on the enhancement of O_3 in the lower free atmosphere and near surface. This study is aimed to present a more comprehensive assessment on the impact of stratospheric intrusion on the enhancement of springtime O_3 in the lower troposphere and then quantify the role of entrainment in surface O_3 enhancement under different categories of synoptic patterns.

The remainder of this paper is organized as follows: A description of the model configurations, the relevant data, and process-analysis method are presented in Section 2. The impacts of stratospheric intrusions on the enhancement of O_3 in the lower free atmosphere and near surface are discussed in Section 3. The major findings are summarized in the final part.

2. Methodology and Data

2.1. Observational and Reanalysis Data

Seventeen years of O_3 sounding data in spring months (i.e., March, April, and May) from 2004 to 2020 were used in our analysis. O_3 soundings were operated routinely by HKO at a frequency of once per week around 1400 local standard time (LST). All surface observational sites and ozonesonde locations are shown in Figure 1. The electrochemical concentration cell 6A developed by Science Pump Corporation with a precision ranging from 3% to 5% was used to measure O_3 partial pressure from the surface to the height of approximately 30 km (e.g., Johnson et al., 2002). Additional variables measured by ozonesonde include temperature, RH, wind speeds, and wind directions.

The fifth-generation atmospheric reanalysis of the European Centre for Medium-Range Weather Forecasts (ECMWF) ERA-5 products is an additional data source to verify the WRF/Chem model performance at the upper levels where observational data are very limited. The ERA-5 products are produced by 4D-Var data assimilation of the ECMWF's Integrated Forecast System. This system includes a four-dimensional variational analysis with a 12-h analysis window (Hersbach et al., 2020). The ERA-5 products such as wind speed, PV, and O₃ with a horizontal resolution of 31 km and 137 vertical layers from the surface up to 80 km AGL are used to perform the data analysis and evaluate the WRF/Chem simulated vertical profiles and upper-level fields. Monthly convective available potential energy (CAPE) retrieved from the ERA-5 products is used to represent the potential of atmospheric convective activities.

Monthly tropopause heights are provided by ERA-5 products. The near real-time (NRT) active fire data retrieved from the measurements of the Moderate Resolution Imaging Spectroradiometer (MODIS) (<https://firms.modaps.eosdis.nasa.gov/map>) are used to track the impacts of biomass burning plumes from South-east Asia on tropospheric O₃ enhancement in Hong Kong during the stratosphere intrusion events. The tropopause folding frequency product is provided by the atmospheric dynamics group at ETH Zürich. According to the definition of the product, the tropopause folds are defined when pseudo-soundings pass through the dynamical tropopauses (the areas with 2 PVU or above) for several times by using ERA-Interim based global analysis data, which are available from 1979 to 2014 (Sprenger et al., 2003).

The ABL heights are defined as the places where the potential temperature gradient reaches the maximum (Heffter, 1980) based on HKO operational sounding data.

2.2. The Model and Configurations

WRF/Chem version 3.9.1 is employed in the study (Grell et al., 2005; LeGrand et al., 2019). The model configurations used in this study are the same as those used in Zhao et al. (2021). We continue to use three nested domains at horizontal grid spacings of 27, 9, and 3 km with their respective grid points of 140 × 130, 130 × 118, and 118 × 106 (Figure 1). Forty-six vertical levels are defined with the top level at 50 hPa. All the primary physics parametrization schemes and emissions inventories used in this study are the same as those used by Zhao et al. (2021). But a convective parameterization is only used for Domains 1 and 2, but not for Domain 3. An upper boundary condition (UBC) scheme (Barth et al., 2012) derived from the Whole Atmosphere Community Climate Model simulations is utilized to generate all the key species in stratosphere for handling with the limitation that stratospheric O₃ formation chemistry is not included in the WRF/Chem (Zhao et al., 2021). An analysis nudging technique is used to reduce model forecast errors of temperature, wind speed, and geopotential height, and eventually improve the accuracy of meteorological simulations.

The initial and lateral boundary meteorological conditions are generated from National Centers for Environmental Prediction analysis data, Final (FNL) Global Data Assimilation System data are available for analysis at an interval of 6-h with a horizontal resolution of 1° and 26 vertical levels spanning from 1,000 to 10 hPa. The initial and lateral conditions of chemical species are produced by interpolating the outputs of the Model for Ozone and Related Chemical Tracers version 4 (Emmons et al., 2010) at the horizontal resolutions of 1.9° × 2.5° with 56 vertical levels into the WRF/Chem model domain grids. The Regional Acid Deposition Model version 2 is used to simulate gas-phase chemistry (Stockwell et al., 1990). Three-day simulations are completed for each case, and the first 24-h simulations are treated as a spin-up run.

2.3. Process Analysis

IPR analysis is a diagnostic tool widely used to quantify relative contributions of individual physical processes and chemical production to spatial and temporal variations in chemical species of interest such as O₃ (e.g., Huang et al., 2005; Jeffries & Tonnesen, 1994).

As an Eulerian grid model, WRF/Chem calculates time rates of change in chemical species concentrations (C_i) at individual grids and each time step through solving the following set of mass continuity equations numerically (Jeffries & Tonnesen, 1994; Jiang et al., 2013)

Table 1

The Total Numbers of Ozone (O₃) Sounding, Total O₃ Enhancement Events, Stratospheric Intrusion Cases, and Intrusion-Associated O₃ Enhancement Events in the Lower Free Troposphere (From the Top of the Atmospheric Boundary Layer to the Height of 4-km Above Ground Level) Over Hong Kong in Spring During 2004–2020

Year	2004	2005	2006	2007	2008	2009	2010	2011	2012	2013	2014	2015	2016	2017	2018	2019	2020	Total
Soundings	16	10	13	11	13	12	12	10	9	9	5	9	13	10	9	12	12	185
O ₃ enhancement events	8	5	3	4	3	4	3	4	4	4	3	6	7	7	5	6	5	81
Intrusion cases	7	4	5	2	3	5	5	4	3	4	2	3	4	2	3	4	3	63
Intrusion-associated O ₃ enhancement events	4	2	1	0	0	2	1	1	0	1	1	1	1	0	2	2	1	20

$$\frac{\partial C_i}{\partial t} = -\left(u \frac{\partial C_i}{\partial x} + v \frac{\partial C_i}{\partial y}\right) - w \frac{\partial C_i}{\partial z} + \frac{\partial}{\partial z} \left(K_e \frac{\partial C_i}{\partial z}\right) + R + D + E, \quad (1)$$

where u , v , and w denote three components of wind speed in x , y , and z directions, respectively; κ is eddy diffusivity. The six terms on the right-hand side in Equation 1 represent horizontal advection, vertical advection, vertical diffusion, chemical reactions (R), dry deposition (D), and emission rate (E), respectively.

As presented in Equation 1, chemical species concentrations are governed by various processes, whereas the models write out instantaneous fields at an interval of one hour without the detailed contributions of individual processes at each integration time step. The configurations of WRF/Chem model are modified to write out the contributions of individual processes to the change of total concentrations at each grid and each hour for a post-processing analysis. The net changes in the total chemical reactions rather than individual chemical reactions are tracked through IPR analysis. With such output information, the contributions by individual processes and net change of chemical reactions to a chemical species (e.g., O₃) can be assessed quantitatively at a given region over a period of interest (e.g., Huang et al., 2005; Zhao et al., 2019).

In this study, the IPR calculations are performed to track the contributions of individual processes especially stratospheric intrusions to the changes in O₃ at different layers in the troposphere over Hong Kong and the surrounding regions (i.e., the innermost domain, D3) during the time window from 11 to 15 LST that matches the launching time of O₃ sounding around 1–2 p.m. LST.

3. Results and Discussion

3.1. Enhancement of Spring O₃ in the Lower Troposphere and Synoptic Patterns

Stratospheric intrusions are important contributors to the enhancement of O₃ in the lower troposphere during spring months (March, April, and May) (Kim & Lee, 2010; Ni et al., 2019; Zhao et al., 2021). O₃ enhancement is defined as the case when O₃ concentrations exceed 70.0 ppbv about 15% higher than climatology means of 61 ppbv at the layer from the top of ABL to 4 km AGL (Zhao et al., 2021). The criteria proposed by Zhao et al. (2021) are modified slightly to identify the stratospheric intrusion events in springtime from 2004 to 2020. They include (a) RH less than 20%, (b) PV higher than 1 PVU (James et al., 2003; Kim & Lee, 2010), (c) O₃ levels with 25% above the climatological mean from tropopause (i.e., 16-km AGL) to 8 km AGL (Van Haver et al., 1996), and (d) upper-level wind speed higher than 20 m s⁻¹ (Antonescu et al., 2013; Rao et al., 2008).

A total of 185 sounding profiles are available in spring months during 2004–2020 (Table 1). With the criteria proposed above, 81 O₃ enhancement events observed in the lower free troposphere (i.e., from the top of the ABL to the height of 4-km AGL) were identified from the O₃ sounding data while 63 stratospheric intrusion events were observed during the study period. Twenty O₃ enhancement events in the lower troposphere were closely associated with the stratospheric intrusions. In other words, 24.7% (20 out of 81) of O₃ enhancement events were largely related to stratospheric intrusion, whereas 31.7% (20 out of 63) of intrusion events (63) led to the enhancement of O₃ in the low troposphere. In the previous research, seasonal mean

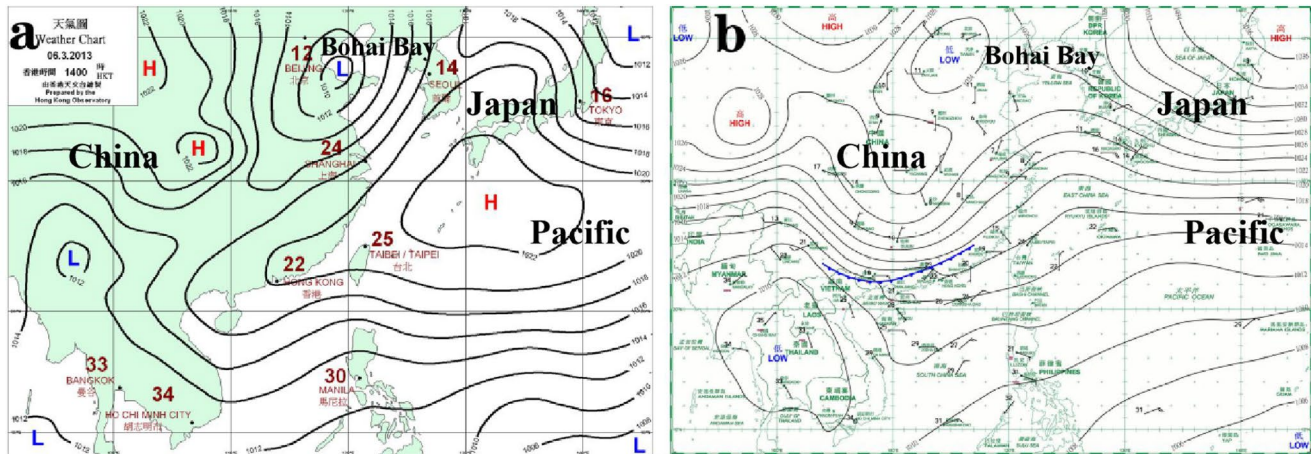


Figure 2. Surface weather charts associated with the low-level tropospheric ozone enhancement in Hong Kong for (a) synoptic pattern “S” on March 6, 2013 and (b) synoptic pattern “F” on March 7, 2018.

tropopause fold frequency distributions showed that the folding occurred preferentially in the subtropics with the maximum frequency of 30% (Sprenger et al., 2003). Thus, stratospheric intrusions played an important role in the substantial enhancement of O_3 concentrations in the lower free troposphere.

Synoptic patterns associated with stratospheric intrusion-driving O_3 enhancements are classified into two categories: Saddle Point or Col (i.e., pattern “S”) and Cold Front (i.e., pattern “F”) (Figure 2). For synoptic pattern “S,” a high-pressure system (anticyclone) was located east of Japan and another high pressure situated over northwest China while two low-pressure systems (L) were located over southwest China and the Bohai bay. For this case, the weather was dominated by relative stable weather conditions with low wind speeds on March 6, 2013 (Figure 2). For synoptic pattern “F” identified on March 7, 2018, a strong cold front with a strong high-pressure system was approaching Hong Kong from the north and the weather was characterized by cloudy or rainy conditions.

As shown in Table 2, 14 and 6 O_3 enhancement events are identified as patterns “S” and “F” by examining the weather maps provided by the HKO. These synoptic patterns are closely associated with the occurrence of O_3 enhancement in the lower free troposphere but need to be connected with the upper-level dynamics.

3.2. Occurrence of Stratospheric Intrusions and Impact on Tropospheric O_3 in Springtime

Tropopause folding is one of the most important physical mechanisms inducing stratospheric intrusion in the subtropical regions (Meloan et al., 2001; Scott & Cammas, 2002) with the upper tropospheric jet stream representing an important physical regime driving tropopause folding (Zhao et al., 2021). The subtropical jet (STJ) is critical for the occurrence of stratospheric intrusions in the subtropical regions. The STJ usually develops at the transition between the Hadley and Ferrel cells driven by solar radiation forcing and Coriolis force (Lachmy & Harnik, 2014). The STJ usually propagates eastward accompanied by Rossby waves. Vertical mixing can be greatly enhanced because of a breaking Rossby wave. According to Zhao et al. (2021) and other studies (Blackmon et al., 1977; Langford, 1999), a large-scale subsidence occurs at the south-hand side of the core of STJ where strong vertical wind shears develop, and such a strong subsidence accompanied by a tropopause folding may bring O_3 -enriched air from the stratosphere downward to the troposphere. However, stratospheric intrusions are often observed in spring rather than in winter and other seasons, whereas the strongest upper-level STJs are observed in winter rather than spring. In this section, we attempt to answer the question why stratospheric intrusions occur in this region in spring rather than in other seasons before we assess the impact of stratospheric intrusions on tropospheric O_3 in Hong Kong.

Figure 3 shows the spatial distributions of seasonal mean wind speeds at the 200-hPa height where the core of the upper tropospheric jet stream is located. The strongest wind speeds are observed in winter (i.e., December, January, and February) and a red band with wind speed higher than 60 m s^{-1} is extending from

Table 2

A Summary of Ozone (O_3) Enhancement Cases Observed in the Lower Free Troposphere (From the Top of Atmospheric Boundary Layer to the Height of 4 km Above Ground Level), Associated Surface Synoptic Patterns, Meteorological Conditions ($T_{2,max}$ and $W_{10,max}$), Surface Maximum O_3 and Lower Tropospheric Maximum O_3 Concentration, and the Maximum Wind Speed at 200-hpa Level in Hong Kong During the Period of 2004–2020

Case (yyyymmdd)	Synoptic pattern	Max. T_2 ($^{\circ}C$)	Max W_{10} (m/s)	Surface max O_3 (ppbv)	Lower tropospheric maximum O_3 concentration (ppbv)	Maximum upper-level wind speed (m/s)
20040324	S	18.9	6.9	59.7	98.8	39.6
20040331	S	19.1	7.3	57.8	98.4	40.3
20040412	S	30.1	3.5	45.9	70.0	32.7
20040510	S	29.6	4.9	63.8	84.7	25.6
20050309	S	22.2	3.9	NA	77.9	47.6
20050323	S	22.9	6.2	NA	78.1	37.8
20060412	F	31.1	4.5	22.7	87.4	30.7
20090408	S	23.3	5.5	77.6	85.3	50.1
20090506	S	25.2	7.5	81.1	85.7	30
20100324	F	25.6	6.3	28.0	86.8	36.8
20110420	F	23.6	6.1	101.5	88.1	36.5
20130306	S	20.9	6.2	83.1	77.8	49.7
20140402	S	19.6	4.2	52.6	88.1	47.7
20150317	S	21.5	6.2	41.3	83.2	28.7
20160414	F	21.5	2.8	33.2	103.8	28.6
20180307	F	20.8	10.6	55.6	72.2	40.6
20180411	F	26.4	5.3	51.0	92.5	42.9
20190320	S	24.7	4.9	38.3	113.1	35.9
20190403	S	25.3	5.6	44.4	120.1	30.8
20200408	S	24.0	5.5	41.2	90.2	53.2
Mean	S	23.4	5.6	57.2	89.4	39.3
Mean	F	24.8	5.9	48.7	88.5	36.0
Mean	Total	23.8	5.7	54.4	92.9	38.3
STDEV	S	3.5	1.2	16.2	13.9	9.1
STDEV	F	2.4	2.8	29.1	11.4	5.4
STDEV	Total	3.5	1.7	20.8	12.7	8.2

Note. NA means the observational data are not available. STDEV, standard deviation.

the northwest Pacific to mainland China and north of Hong Kong. The range of red regions with high wind speed becomes much smaller in spring. The STJ band moves northward and its intensity becomes much weaker in summer. The STJ tends to strengthen and moves back to a low latitude in the fall. The seasonal movement and intensity of STJ may explain why stratospheric intrusions do not occur in summer and fall over Hong Kong but cannot explain why they do not occur in winter. A similar pattern is also found in tropopause folding frequency in different seasons (Figure 4). A high tropopause fold frequency is noticed along 30°N in winter and spring with the maximum value exceeding 22% and 18%, indicating a higher potential of stratospheric intrusion occurring in this region. A clear linkage is noticed between the seasonal movement and intensity of STJ and tropopause fold frequency.

According to other studies (e.g., Gray, 2003; Hsu et al., 2005; Nakamura, 1992; Q. Tang et al., 2011), occurrence and intensification of stratospheric intrusion in spring are closely associated with strengthening upper troposphere baroclinic activities such as cutoff low and tropopause folding. Here, we use the CAPE as

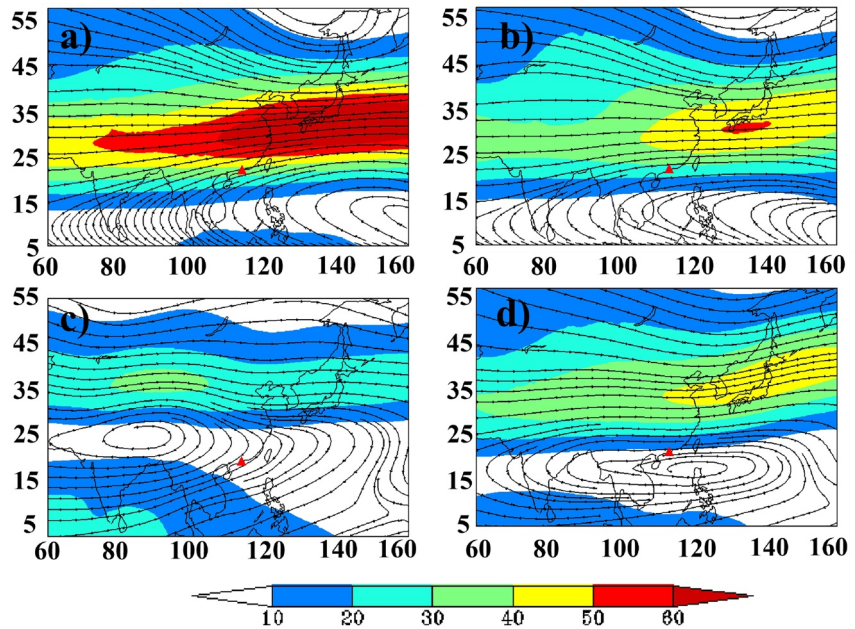


Figure 3. Seasonal mean wind fields at the 200-hPa level derived from the ERA-5 data for the period 2004–2020. (a) Winter, (b) spring, (c) summer, and (d) autumn (red triangle represents the Hong Kong location).

the indicator to represent convective activity. The CAPE is a good indicator of representing the potential of the atmospheric convective activity (Schlemmer et al., 2010). As shown in Figure 5, the CAPE is much higher in spring and summer than in winter. Thus, an index tropopause fold frequency-CAPE (TC) is defined as the integrated product of tropopause folding frequency with CAPE. A higher value in spring indicates that

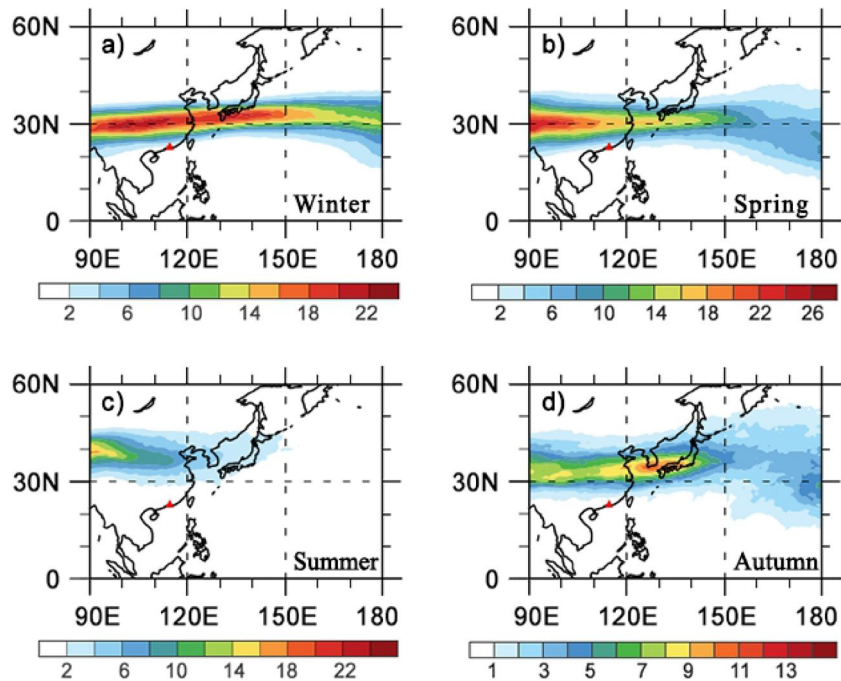


Figure 4. Seasonal mean of tropopause folds frequency during 2004–2014 (a) winter, (b) spring, (c) summer, and (d) autumn (red triangle represents the Hong Kong location). This product provided by the atmospheric dynamics group at ETH Zürich, <http://eraiclim.ethz.ch/>.

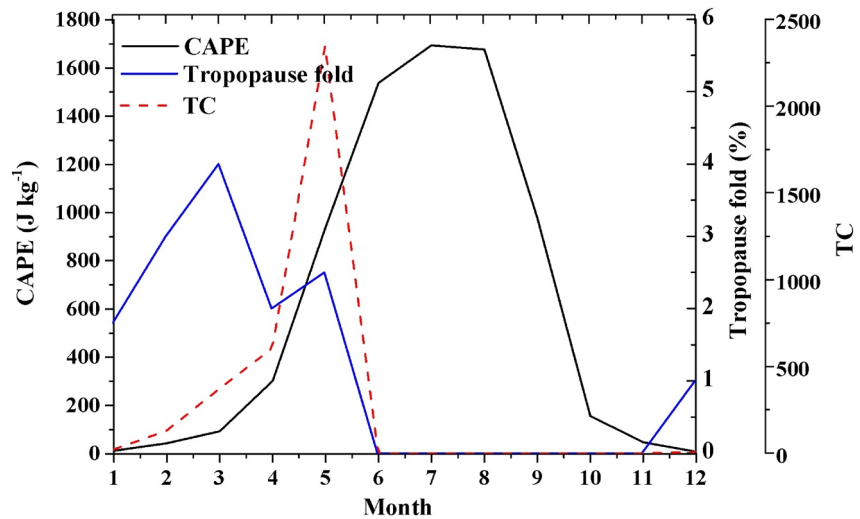


Figure 5. Monthly mean of convective available potential energy (CAPE) between 2004 and 2014 (black solid line), tropopause fold frequency (blue solid line), and tropopause fold frequency-CAPE (TC) (red dashed line). The tropopause fold frequency was provided by the atmospheric dynamics group at ETH Zürich, <http://eraiclim.ethz.ch/>.

the occurrences of stratospheric intrusions are highly related to the integrated effect of tropopause folding and troposphere convective activities in subtropical regions like Hong Kong.

3.3. Characteristics of Two Representative O₃ Enhancement Events Under Two Different Synoptic Patterns

Two representative stratospheric intrusion-associated O₃ enhancement events are presented to compare the characteristics of stratospheric intrusion process-driven O₃ enhancement under two different categories of synoptic patterns (see Figure 2). They include Case A, a representative of synoptic pattern “S” on March 6, 2013, and Case B, a representative of synoptic pattern “F” on March 7, 2018. Figure 6 further displays a comparison of vertical profiles between WRF/Chem simulations (bold dashed line), ERA-5 reanalysis data (thin dashed line), and sounding observations of O₃, RH, wind speeds, and temperature for the two intrusion events. The ABL and tropopause heights are included in support of the analysis. The statistical evaluations of simulated O₃ and meteorological fields are presented in Tables S1 and S2, respectively. Overall, the WRF/Chem simulations show a reasonable performance in capturing vertical distributions of individual variables for both cases with a correlation coefficient (*R*) higher than 0.8.

For Case A, while O₃-enriched air with concentrations higher than 70.0 ppb was transported from the stratosphere (above 16 km AGL) downward to the lower troposphere (Figure 6a), RH was less than 25% across the layers from the tropopause to the height at 6.0 km AGL (Figure 6c). This indicates that a stratospheric intrusion event was taking place, and O₃ was enhanced across the entire troposphere including the ABL.

In addition, it is noticed that the ABL height for the case studies associated with synoptic pattern “F” is usually lower than that of the cases associated with the synoptic pattern “S” (i.e., 0.9 vs. 1.8 km) (Figures 6g and 6h). A similar phenomenon was also observed by Sinclair et al. (2010).

The WRF/Chem model underpredict O₃ concentrations from the tropopause to the middle troposphere (i.e., 8–18 km) in both cases. The underpredictions of O₃ in the upper troposphere are likely related to inaccurate UPCs, missing lightning NO_x, incomplete chemistry, and insufficient vertical resolution (e.g., Henderson et al., 2011). In addition, the ERA-5 reanalysis data showed much higher O₃ concentrations than both WRF/Chem simulations and O₃ sounding from the middle of troposphere to the tropopause. The difference could be partially related to the different resolutions between WRF/Chem simulations (3 km in horizontal and 46 vertical levels from surface to 50 hPa) and the one used for generating the reanalysis product (31 km in horizontal and 137 levels from the surface up to 80 km).

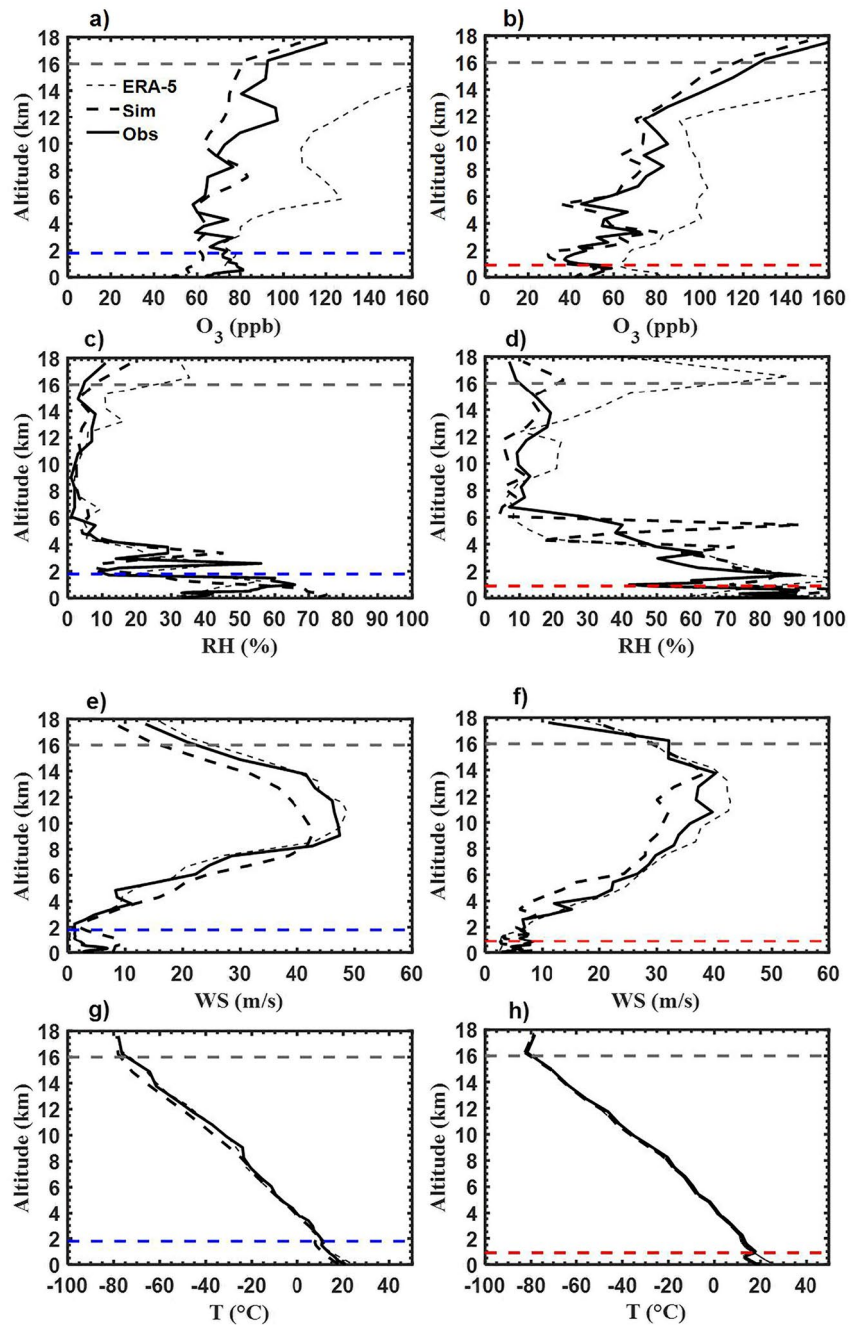


Figure 6. A comparison of vertical profiles from Weather Research and Forecasting/Chemistry simulations (bold dashed line), ERA-5 (thin dashed line), and sounding observations (solid line) at 1400 local standard time for (a and b) ozone (O_3), (c and d) relative humidity (RH), (e and f) wind speed (WS, m/s), and (g and h) temperature on March 6, 2013, (left panel) and on March 7, 2018 (right panel) (gray line: tropopause height; blue line: atmospheric boundary layer height (ABLH) on March 6, 2013; red line: ABLH on March 7, 2018).

In order to further quantify the impact of stratospheric intrusions on O_3 enhancement in the lower free troposphere, the remaining eighteen-case simulations are completed to support the IPR analysis. The statistical evaluations of all the simulated cases are presented in Table S3. Zhao et al. (2021) have demonstrated the capability of WRF/Chem in simulating the stratospheric intrusion events (1). We further evaluate the model performance on O_3 simulations in the low (i.e., 2.5–4 km), middle (i.e., 4–10 km), and upper levels of the troposphere (i.e., 10–18 km) (Table S4). Overall, the WRF/Chem shows a realistic performance in

Table 3

Integrated Process Rate Analysis on Contributions of Three Dominant Processes (Vertical, Horizontal Transport, and Chemical Production) to the Total Changes of Ozone (O_3) in the Lower Free Troposphere for the Period of 11:00–15:00 LST for 20 O_3 Enhancement Events

Cases (yyyymmdd)	Vertical (ppbv h ⁻¹)	Horizontal (ppbv h ⁻¹)	Chemical (ppbv h ⁻¹)	Net (ppbv h ⁻¹)	Synoptic pattern
20040324	20.5	-16.7	-0.2	3.6	S
20040331	21.7	-14.1	-0.2	7.4	S
20040412	19.2	-12.7	-0.3	6.2	S
20040510	18.9	-15.1	-0.1	3.7	S
20050309	19.3	-14.1	-0.3	4.6	S
20050323	19.5	-14.1	-0.2	5.2	S
20060412	23.1	-18.7	-0.3	4.1	F
20090408	24.2	-20.1	-0.3	3.8	S
20090506	20.1	-17.2	-0.3	2.6	S
20100324	28.4	-20.2	-0.2	8	F
20110420	25.4	-22.3	-0.3	2.8	F
20130306	27	-23.1	-0.5	4.4	S
20140402	28.3	-20.5	-0.2	7.6	S
20150317	26.5	-21.2	-0.2	5.1	S
20160414	22.5	-19.2	-0.3	3	F
20180307	26.3	-19.7	-0.4	6.2	F
20180411	27.3	-21.2	-0.2	5.9	F
20190320	28.2	-20.5	-0.3	7.4	S
20190403	20.6	-13.3	-0.2	7.1	S
20200408	22.3	-16.8	-0.3	5.2	S
Mean	22.6	-17.3	-0.3	5.3	S
Mean	25.5	-20.2	-0.3	5	F
Mean	23.5	-18.2	-0.3	5	Total

simulating both meteorological fields and O_3 at the upper levels of troposphere after the key chemical species in the stratosphere are adjusted with the global atmospheric chemical model outputs (Zhao et al., 2021).

3.4. Impact of Stratospheric Intrusions on O_3 Changes in the Lower Troposphere

In this section, IPR analyses are performed to quantify the contributions of stratospheric intrusion to O_3 enhancement in the layer from the top of the ABL to 4 km AGL over Domain 3 during the period of 11:00–15:00 LST when O_3 formation was the most active and O_3 soundings were launched routinely (i.e., 14:00 LST).

As shown in Figure 6, the maximum wind speed (47.4 m s⁻¹) at the upper level was higher for case A (i.e., synoptic pattern S) than case B (i.e., synoptic pattern F) (40.2 m s⁻¹). The height of STJ core location of case A was lower than that of case B, indicating that stronger wind shear under the STJ core can promote stronger stratospheric intrusions for case A.

It is noticed that the vertical atmospheric stability plays a critical role in determining whether O_3 -enriched air can be transported downward to the ABL. As shown in Figure S1, a vertical gradient of 0.45°C/100 m or no obvious inversion was observed at the top of the ABL on March 6 for case A, whereas a strong inversion with a lapse rate of 1.7°C/100 m was seen above the top of the ABL (i.e., 900-m AGL). The inversion effectively constrains the downward transport of O_3 -enriched air from the free atmosphere to the ABL for Case B.

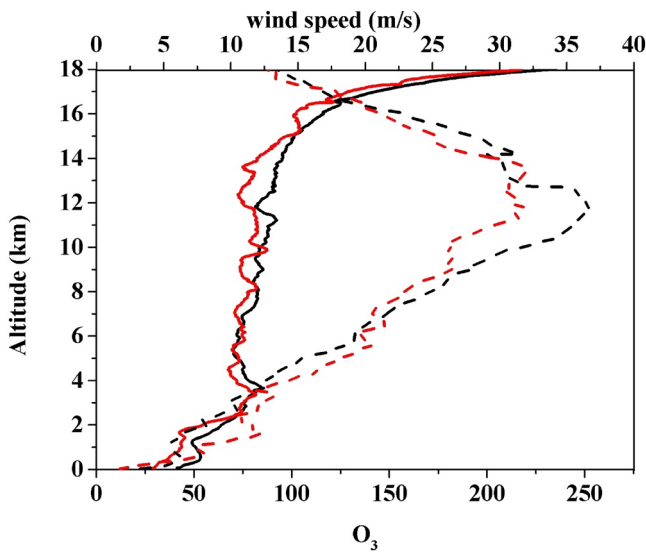


Figure 7. A comparison of observed vertical wind (dashed line) and ozone (O_3) (solid line) profiles in spring during 2004–2020 (black line: synoptic pattern “S”; red line: synoptic pattern “F”).

Twenty simulations with IPR analyses are presented to quantify the impact of stratospheric intrusions on O_3 enhancement for the cases associated with the two types of surface synoptic patterns (Table 3). The average of maximum O_3 concentrations associated with synoptic pattern “F” was usually lower than that of synoptic pattern “S” during the study period (72.2 vs. 77.8 ppbv). Meanwhile, the IPR results showed that the net change of O_3 of the cases associated with synoptic pattern “F” was lower than that of the cases associated with the synoptic pattern “S” (i.e., 5 vs. 5.3 ppbv h^{-1}). This can be further illustrated by the vertical profiles of O_3 and wind speeds (Figures 6 and 7). Our results demonstrate that the means, the maximum, and the minimum values associated with synoptic pattern “F” are lower than that of the cases associated with the synoptic pattern “S.”

As seen in Table 3, the vertical transport contributed the significant O_3 enhancement in the lower free troposphere during the stratospheric cases. Consequently, the IPR analyses clearly illustrated an important role of stratospheric intrusions in the enhancement of O_3 in the lower troposphere, which accounted for 24.7% of O_3 enhancement of total simulated cases, while other studies highlighted the contributions of regional transport from Southeast Asia where biomass burning was active during springtime (e.g., C. Y. Chan & Chan, 2000; L. Y. Chan et al., 2000).

The IPR is used to quantify the contributions of individual processes to the change in O_3 over the predefined region during a certain period but is not able to identify the sources of forecast errors explicitly. The technique uses a simple separation of individual processes and does not account for the interactions among them, which may cause some uncertainties. This is the reason that the IPR analysis shows much larger contributions of horizontal and vertical transports than other terms such as

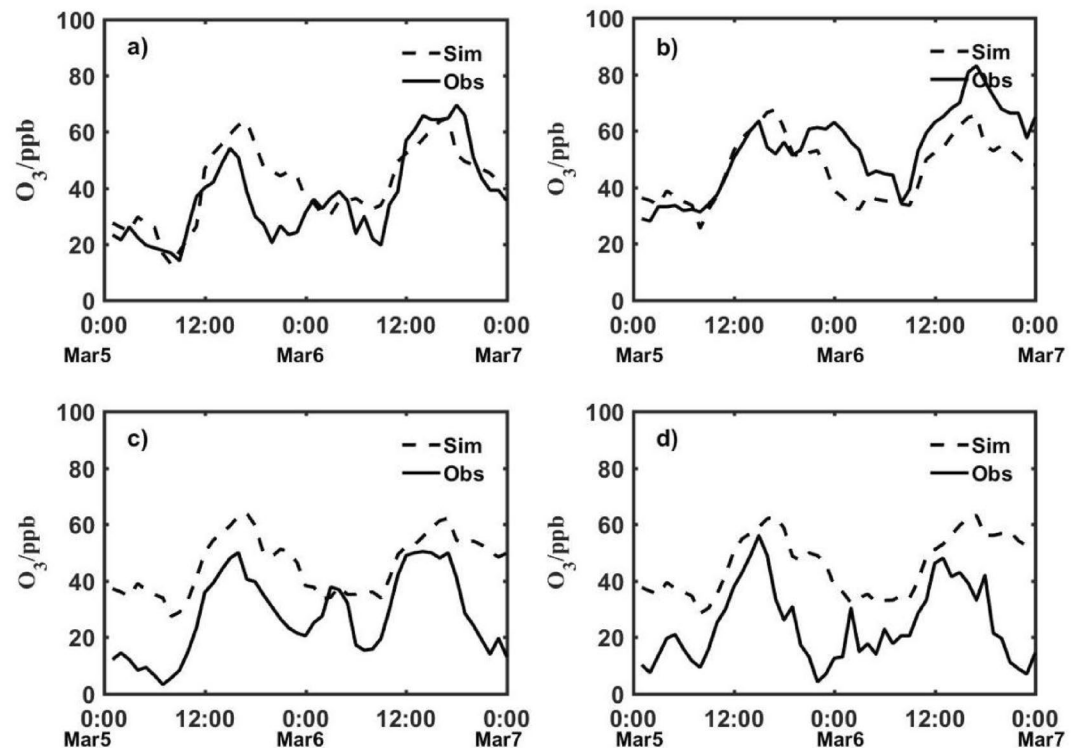


Figure 8. A comparison of simulated surface ozone (O_3) with observation during March 5–6, 2013 at (a) Sha Tin, (b) Tap Mun, (c) Taiipo, and (d) Tung Chung.

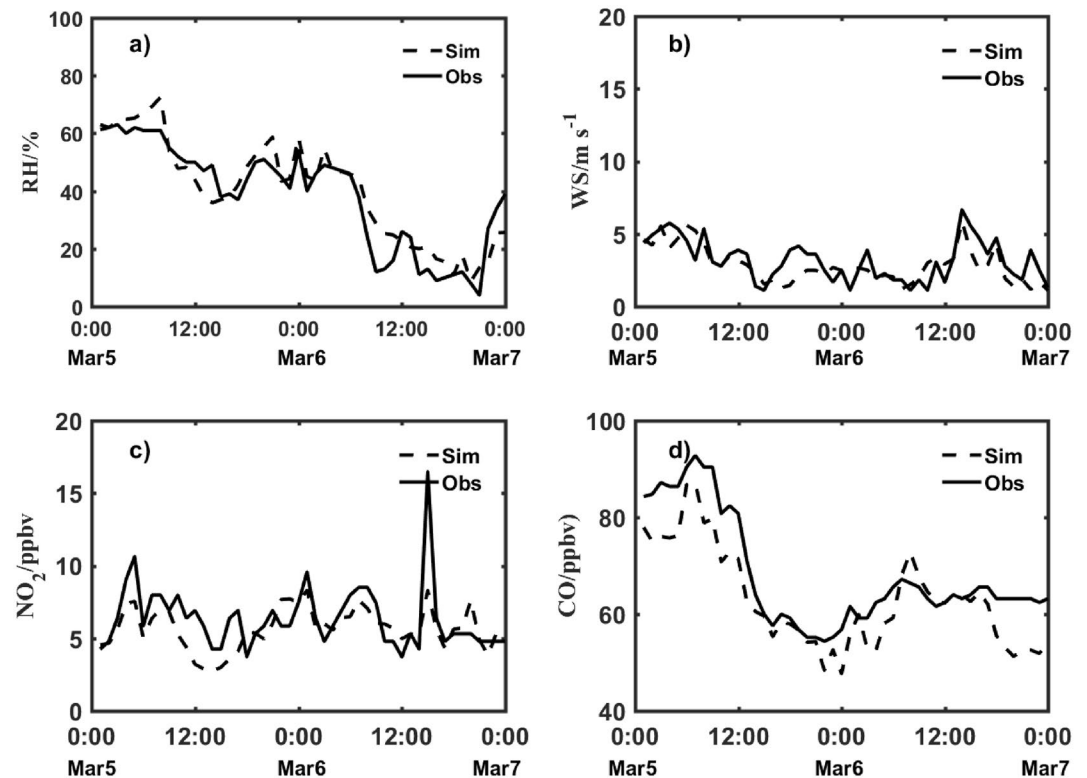


Figure 9. Simulated (dashed lines) and observed (solid lines) surface parameters at Tap Mun station during March 5–6, 2013: (a) relative humidity, (b) wind speed, (c) NO_2 concentration, and (d) carbon monoxide (CO) concentration.

photochemical reactions. In addition, other factors such as uncertainties of emissions, gas-phase chemical mechanism, and physical parameterization schemes could be part of the reasons causing the uncertainty of IPR analysis.

We further investigate the distinction between two different categories of synoptic patterns in spring during 2004–2020. The mean of the maximum wind speeds exceeded 36.5 m s^{-1} in the layer of 10–12 km altitude under the synoptic pattern “S,” which were higher than those (31.5 m s^{-1}) under the synoptic pattern “F” (Figure 7). We have calculated the standard deviation (STDEV) of the maximum wind speeds for the two synoptic patterns and the results are added in Table 2. The range of the maximum wind speeds are $25.6\text{--}53.2 \text{ m s}^{-1}$ and $28.6\text{--}42.9 \text{ m s}^{-1}$ for synoptic patterns “S” and “F,” respectively. The STDEV of the maximum wind speeds for synoptic pattern “S” and “F” are 9.1 and 5.4 m s^{-1} , respectively. According to the analysis, the difference in the maximum wind speeds of the STJ is not the key factor causing the difference in O_3 concentrations in the O_3 -enhancement layer in the lower troposphere, that is, the layer of 2–4 km above the AGL. Instead, the difference in O_3 concentrations in the enhancement layer (i.e., the layer above the ABL) is mainly attributed to the atmospheric stabilities of the layer above the ABL. The intensity of stratospheric intrusions is relatively stronger under patterns “S” due to the higher upper-level wind speed; thus, higher tropospheric O_3 (i.e., 12 km) was observed at upper levels.

3.5. Impact of Stratospheric Intrusions on Surface O_3

As presented above, stratospheric intrusions may bring O_3 -enriched air downward to the lower free atmosphere, leading to substantial O_3 enhancement within the layers from the top of the ABL to the height of 3–4-km AGL (Figure 7). Now, we turn our attention to assess the impact of stratospheric intrusion on O_3 concentrations near the surface through entrainment.

Figure 8 shows a comparison of simulated O_3 with observed surface O_3 at four monitoring sites operated by the Hong Kong Environmental Protection Department on March 5–7, 2013, a representative case of synop-

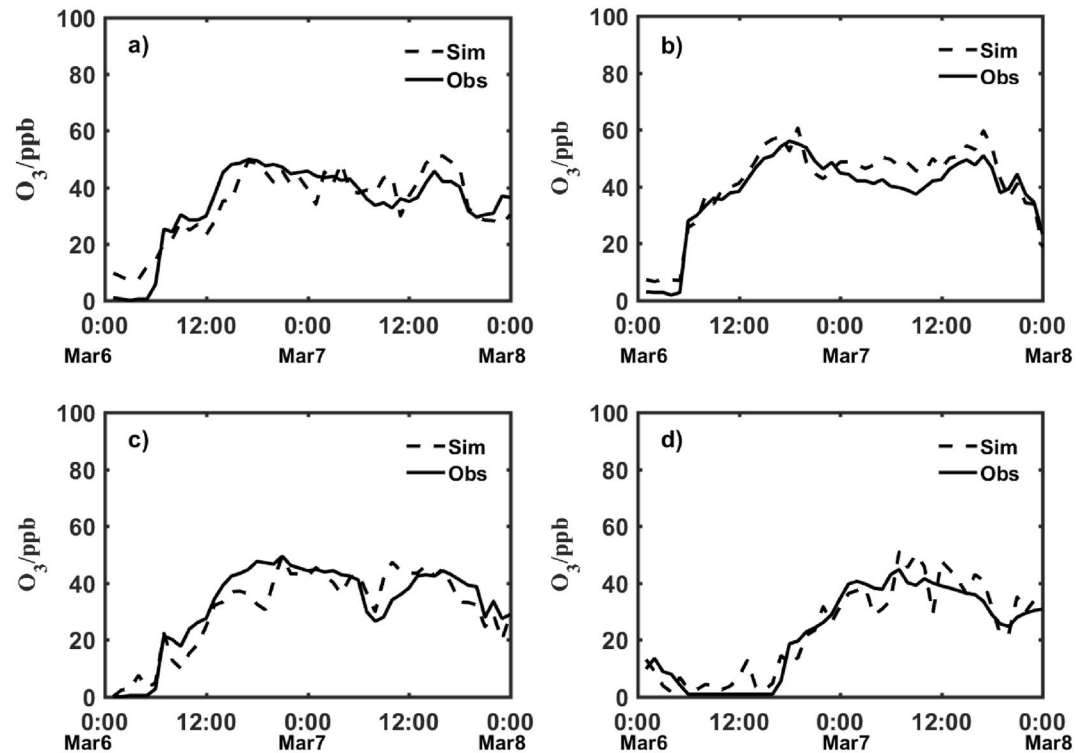


Figure 10. A comparison of simulated surface ozone (O_3) with observation during March 6–7, 2018 at (a) Sha Tin, (b) Tap Mun, (c) Taipo, and (d) Tung Chung.

tic pattern “S.” Overall, the model was able to capture diurnal variation pattern and spatial variability with slight underprediction at Sha Tin (see Figure 1 for site location) and Tap Mun (a and b) on March 6, a rural site located at the northeast of Hong Kong, about 30 km from the downtown, but slightly overpredicted O_3 levels at Taipo and Tung Chung (c and d). The statistical calculations are presented in Tables S5–S7 to evaluate the model performance. As a rural site, the concentrations at Tap Mun represented the impact of regional transport from the Pearl River Delta and a large subsidence such as stratospheric intrusion. O_3 levels were elevated to above 83.0 ppbv on March 6 when surface weather was dominated by synoptic pattern “S.” Both RH and CO concentrations were extremely low (less than 20% for RH and 65.0 ppbv for CO) (Figure 9) while the prevailing winds were southeasterly on March 5 and 6, 2013 (Figure S2). The CO concentration was about 41% lower than climatology means (i.e., 111 ppbv in March) (Zahn et al., 2002). Those were the evidence that O_3 -enriched air originated in the stratosphere and reached near the surface. It should be noted that the model did not pick up the large spike in NO_2 on March 6 (Figure 9c). The large difference between the observations and the simulations on March 6 could be related to the uncertainties of emissions or other factors (e.g., meteorological factors).

In contrast, the observed maximum hourly surface O_3 concentrations for Case B were much lower than that of Case A (51.0 vs. 81.0 ppbv) at Tap Mun site (Figure 10). This indicates that stratospheric intrusion has very limited impact on O_3 near the surface for the cases associated with synoptic pattern “F” (Figure S1). It can be explained by high RH (81%) and high CO concentrations (336 ppbv) observed at Tap Mun on March 7, 2018 (Figure 11). High RH is favorable for wet scavenging that may reduce ambient O_3 levels further (Case B). In addition, a strong inversion layer with a lapse rate of $1.7^\circ\text{C}/100\text{ m}$ observed above the ABL (i.e., 900 m AGL) blocked the O_3 -enriched air entering the ABL.

Another possible reason for the lower O_3 concentration on March 7, 2018 (i.e., Case B) is that the observed maximum hourly surface NO_2 concentrations were much lower than that on March 6, 2013 (i.e., Case A) (i.e., 10.3 ppbv of Case B vs. 16.1 ppbv of Case A) at the Tap Mun site (Figures 9c and 11c). As the Tap Mun

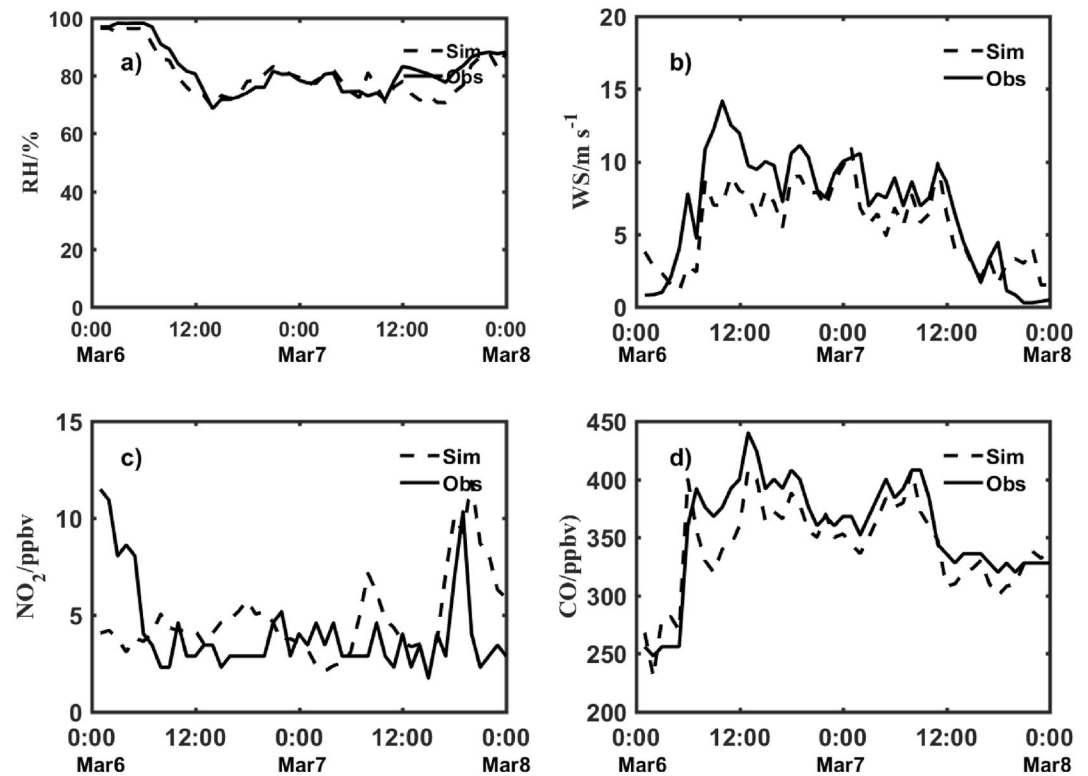


Figure 11. Simulated (dashed lines) and observed (solid lines) surface parameters at Tap Mun station during March 6–7, 2018: (a) relative humidity (RH), (b) wind speed (WS), (c) NO_2 concentration, and (d) carbon monoxide (CO) concentration.

site is a rural site, O_3 production dominated by the NO_x -limited regime and ambient levels of O_3 showed positive dependence on NO_2 concentrations.

To exclude the possible contributor of biomass burning plumes from Southeast Asia, the NRT active fire data within 3 h of satellite observation from the MODIS data are used to investigate the impacts of biomass burning plumes from Southeast Asia on tropospheric O_3 enhancement in Hong Kong during the stratosphere intrusion events. As seen in Figure 12, air mass was not transported from fire active areas at 500, 2,000, and 4,000 m, which further indicated that the long-range transport of biomass burning was not a contributor to O_3 enhancement over Hong Kong since very few fire points were observed in those fire source locations during the events. Hence, it is concluded that O_3 enhancement over Hong Kong in these two cases were mainly associated with stratospheric intrusions rather than the contributions of biomass burning plumes from Southeast Asia.

4. Conclusions

In this study, 17 years of O_3 sounding data are analyzed to identify stratospheric intrusion-associated O_3 enhancement events in the lower free troposphere in Hong Kong during springtime from 2004 to 2020. Synoptic patterns are classified through careful examination of the weather maps associated with stratospheric intrusion-related enhancement of O_3 in the lower troposphere. Data analyses are presented to understand the reasons that stratospheric intrusions occur in spring rather than in other seasons. WRF/Chem model with the IPR is performed to quantify the impacts of stratospheric intrusions on O_3 enhancement in the lower free atmosphere and near surface.

A total of 185 O_3 sounding profiles from 2004 to 2020 are included in the data analysis. Among them, 20 cases with O_3 enhancement in the lower troposphere were related to stratospheric intrusions and two types

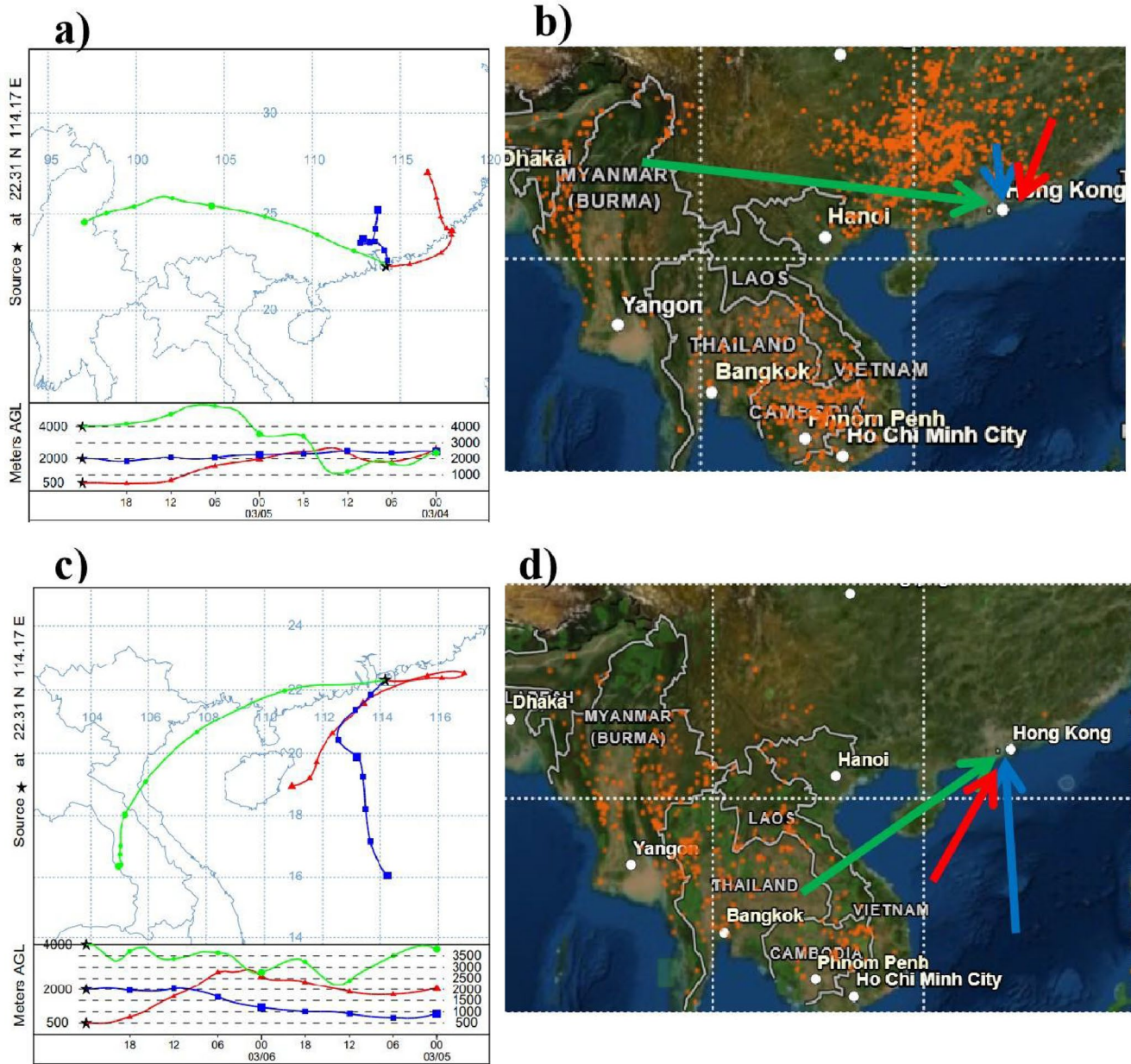


Figure 12. Backward air mass trajectories and fire map provided by NOAA air resources laboratory (<https://www.ready.noaa.gov/>) and Fire Information for Resource Management System from NASA (<https://firms.modaps.eosdis.nasa.gov/>) on (a and b) March 6, 2013 and (c and d) March 7, 2018.

of synoptic patterns: saddle point (“S”) and cold front (“F”). Synoptic patterns “S” and “F” accounted for 70.0% and 30.0% of total stratospheric intrusion-associated lower tropospheric O₃ enhancement events.

The tropopause folding and troposphere convective activities are considered as two key factors accounting for the occurrences of stratospheric intrusion during springtime in Hong Kong. An index, TC, as an integrated effect of the CAPE with tropopause folding frequency is proposed to represent the occurrence of stratospheric intrusion in springtime over the subtropical regions like Hong Kong.

The IPR denotes that vertical transport plays a critical role in O₃ enhancement in the lower free troposphere. The impact of intrusion on O₃ enhancement in the lower troposphere is not only dependent on the intensity of intrusion but also the meteorological conditions in the lower troposphere. The net change in O₃ for the cases associated with synoptic pattern “F” was lower than that of the cases associated with the synoptic

pattern “S.” Our results underscore that stratospheric intrusions play an important role in the substantial enhancement of O₃ in the lower troposphere while the biomass burning from Southeast Asia is identified by other studies as another major source causing O₃ enhancement events in the lower troposphere over Hong Kong.

O₃-enriched air can be transported downward to the ABL and exerts an important impact on surface O₃ for the synoptic pattern “S.” In contrast, O₃-enriched air was blocked at the layer due to the constraint of the stable atmospheric layer at the top of the ABL and the impact on O₃ near the surface was very limited for surface synoptic pattern “F.”

Our results suggest that the impact of the stratosphere intrusion should be considered when anthropogenic emission control strategies are developed to reduce surface O₃ concentrations effectively.

Data Availability Statement

The WRF/Chem model code was downloaded from <http://www2.mmm.ucar.edu/wrf>. The anthropogenic emission data were obtained from <http://www.meicmodel.org/>. The FNL data files can be downloaded from the website (<https://rda.ucar.edu/datasets/ds083.2/index.html>). The ERA-5 reanalysis data can be downloaded from <https://www.ecmwf.int>. The data in this paper can be made available to other researchers through correspondence with hjpfwj@gmail.com.

References

- Akritidis, D., Pozzer, A., Zanis, P., Tyrllis, E., Škerlak, B., Sprenger, M., & Lelieveld, J. (2016). On the role of tropopause folds in summertime tropospheric ozone over the eastern Mediterranean and the Middle East. *Atmospheric Chemistry and Physics*, 16, 14025–14039. <https://doi.org/10.5194/acp-16-14025-2016>
- Antonescu, B., Vaughan, G., & Schultz, D. M. (2013). A five-year radar-based climatology of tropopause folds and deep convection over Wales, United Kingdom. *Monthly Weather Review*, 141, 1693–1707. <https://doi.org/10.1175/mwr-d-12-00246.1>
- Barrett, B. S., Raga, G. B., Retama, A., & Leonard, C. (2019). A multi-scale analysis of the tropospheric and stratospheric mechanisms leading to the March 2016 extreme surface ozone event in Mexico City. *Journal of Geophysical Research: Atmospheres*, 8, 4782–4799. <https://doi.org/10.1029/2018JD029918>
- Barth, M. C., Lee, J., Hodzic, A., Pfister, G., Skamarock, J., Worden, J., et al. (2012). Thunderstorms and upper troposphere chemistry during the early stages of the 2006 North American Monsoon. *Atmospheric Chemistry and Physics*, 12, 11003–11026. <https://doi.org/10.5194/acp-12-11003-2012>
- Blackmon, M. L., Wallace, J. M., Lau, N.-C., & Mullen, S. L. (1977). An observational study of the northern hemisphere wintertime circulation. *Journal of the Atmospheric Sciences*, 34(7), 1040–1053. [https://doi.org/10.1175/1520-0469\(1977\)034<1040:AOSOTN>2.0.CO;2](https://doi.org/10.1175/1520-0469(1977)034<1040:AOSOTN>2.0.CO;2)
- Carmichael, G., Uno, I., Phadnis, M. J., Zhang, Y., & Sunwoo, Y. (1998). Tropospheric ozone production and transport in the springtime in East Asia. *Journal of Geophysical Research*, 103, 10649–10671. <https://doi.org/10.1029/97jd03740>
- Chan, C. Y., & Chan, L. Y. (2000). Effect of meteorology and air pollutant transport ozone episodes at a subtropical Asian city, Hong Kong. *Journal of Geophysical Research*, 105, 20707–20724. <https://doi.org/10.1029/2000jd900140>
- Chan, K. L. (2017). Biomass burning sources and their contributions to the local air quality in Hong Kong. *The Science of the Total Environment*, 596–597, 212–221. <https://doi.org/10.1016/j.scitotenv.2017.04.091>
- Chan, L. Y., Chan, C. Y., Liu, H. Y., Christopher, S., Oltmans, S. J., & Harris, J. M. (2000). A Case study on the biomass burning in Southeast Asia and enhancement of tropospheric ozone over Hong Kong. *Geophysical Research Letters*, 27, 1479–1482. <https://doi.org/10.1029/1999gl010855>
- Cooper, O. R., Parrish, D. D., Stohl, A., Trainer, M., Nédélec, P., Thouret, V., et al. (2010). Increasing springtime ozone mixing ratios in the free troposphere over western North America. *Nature*, 463, 344–348. <https://doi.org/10.1038/nature08708>
- Ding, A., & Wang, T. (2006). Influence of stratosphere-to-troposphere exchange on the seasonal cycle of surface ozone at Mount Waliguan in western China. *Geophysical Research Letters*, 33, L03803. <https://doi.org/10.1029/2005gl024760>
- Emmons, L. K., Walters, S., Hess, P. G., Lamarque, J.-F., Pfister, G. G., Fillmore, D. et al. (2010). Description and evaluation of the model for ozone and related chemical tracers, version 4 (MOZART-4). *Geoscientific Model Development*, 3, 43–67. <https://doi.org/10.5194/gmd-3-43-2010>
- Fowler, D., Flechard, C., Cape, J. N., Storeton-West, R. L., & Coyle, M. (2001). Measurements of ozone deposition to vegetation quantifying the flux, the stomatal and non-stomatal components. *Water, Air, and Soil Pollution*, 130, 63–74. <https://doi.org/10.1023/a:1012243317471>
- Frey, W., Schofield, R., Hoor, P., Kunkel, D., Ravagnani, F., Ulanovsky, A., et al. (2015). The impact of overshooting deep convection on local transport and mixing in the tropical upper troposphere/lower stratosphere (UTLS). *Atmospheric Chemistry and Physics*, 15, 6467–6486. <https://doi.org/10.5194/acp-15-6467-2015>
- Ganguly, N. D. (2012). “Influence of stratospheric intrusion on the surface ozone levels in India”. *ISRN Meteorology*, 2012, 7. <https://doi.org/10.5402/2012/625318>
- Gray, S. L. (2003). A case study of stratosphere to troposphere transport: The role of convective transport and the sensitivity to model resolution. *Journal of Geophysical Research*, 108, D18. <https://doi.org/10.1029/2002JD003317>
- Grell, G. A., Peckham, S. E., Schmitz, R., McKeen, S. A., Frost, G., Skamarock, W. C., & Eder, B. (2005). Fully coupled “online” chemistry within the WRF model. *Atmospheric Environment*, 39, 6957–6975. <https://doi.org/10.1016/j.atmosenv.2005.04.027>
- Han, H., Liu, J., Yuan, H., Wang, T., Zhuang, B., & Zhang, X. (2019). Foreign influences on tropospheric ozone over East Asia through global atmospheric transport. *Atmospheric Chemistry and Physics*, 19, 12495–12514. <https://doi.org/10.5194/acp-19-12495-2019>

Acknowledgments

The ozonesonde data are provided by the World Ozone and Ultraviolet Radiation Data Centre (<https://woudc.org/home.php>). The surface O₃ data are provided by the Hong Kong Environmental Protection Department (<https://cd.epic.epd.gov.hk/EPICDI/air/station/>). The Surface weather charts are provided by the Hong Kong Observatory (http://envf.ust.hk/data-view/hko_wc/current/). The research was supported jointly by the National Natural Science Foundation of China (No. 42105164), the China Postdoctoral Science Foundation (2020M682713), the National Natural Science Foundation of China (No. 91644221), the Research Fund Program of Guangdong-Hong-kong-Macau Joint Laboratory of Collaborative Innovation for Environmental Quality (GHML2021-501), the Xianyang major science and technology projects (2017K01-35), and the National Natural Science Foundation of China (Grant 41575009).

- Heffter, J. L. (1980). *Transport layer depth calculations*. Proceedings of 2nd Joint Conference on Applications of Air Pollution Modelling, American Meteorological Society (Vol. 61, pp. 787–791). <https://doi.org/10.1175/1520-0477-61.8.787>
- Henderson, B. H., Pinder, R. W., Crooks, J., Cohen, R. C., Hutzell, W. T., Sarwar, G., et al. (2011). Evaluation of simulated photochemical partitioning of oxidized nitrogen in the upper troposphere. *Atmospheric Chemistry and Physics*, 11(8), 275–291. <https://doi.org/10.5194/acp-11-275-2011>
- Hersbach, H., Bell, B., Berrisford, P., Hirahara, S., Horányi, A., Muñoz-Sabater, J., et al. (2020). The ERA5 global reanalysis. *Quarterly Journal of the Royal Meteorological Society*, 146, 1999–2049. <https://doi.org/10.1002/qj.3803>
- Hsu, J., Prather, M. J., & Wild, O. (2005). Diagnosing the stratosphere-to-troposphere flux of ozone in a chemistry transport model. *Journal of Geophysical Research*, 110, D19305. <https://doi.org/10.1029/2005JD006045>
- Huang, J., Fung, J. C. H., Lau, A. K. H., & Qin, Y. (2005). Numerical simulation and process analysis of typhoon-related ozone episodes in Hong Kong. *Journal of Geophysical Research*, 110. <https://doi.org/10.1029/2004jd004914>
- Jaeglé, L., Wood, R., & Wargan, K. (2017). Multiyear composite view of ozone enhancements and stratosphere-to-troposphere transport in dry intrusions of northern hemisphere extratropical cyclones. *Journal of Geophysical Research: Atmospheres*, 122, 13436–13457. <https://doi.org/10.1002/2017JD027656>
- James, P., Stohl, A., Forster, C., Eckhardt, S., Seibert, P., & Frank, A. (2003). A 15-year climatology of stratosphere-troposphere exchange with a Lagrangian particle dispersion model: 1. Methodology and validation. *Journal of Geophysical Research*, 108(D12), 8519. <https://doi.org/10.1029/2002JD002637>
- Jeffries, H. E., & Tonnesen, S. (1994). A comparison of two photochemical reaction mechanisms using mass balance and process analysis. *Atmospheric Environment*, 28, 2991–3003. [https://doi.org/10.1016/1352-2310\(94\)90345-x](https://doi.org/10.1016/1352-2310(94)90345-x)
- Jian, Y., & Fu, T.-M. (2014). Injection heights of springtime biomass-burning plumes over peninsular Southeast Asia and their impacts on long-range pollutant transport. *Atmospheric Chemistry and Physics*, 14, 3977–3989. <https://doi.org/10.5194/acp-14-3977-2014>
- Jiang, Z., Liu, Z., Wang, T., Schwartz, C. S., Lin, H., & Jiang, F. (2013). Probing into the impact of 3DVAR assimilation of surface PM10 observations over China using process analysis. *Journal of Geophysical Research: Atmospheres*, 118, 6738–6749. <https://doi.org/10.1002/jgrd.50495>
- Johnson, B. J., Oltmans, S. J., Vömel, H., Smit, H. G. J., Deshler, T., & Kröger, C. (2002). Electrochemical concentration cell (ECC) ozone-sonde pump efficiency measurements and tests on the sensitivity to ozone of buffered and unbuffered ECC sensor cathode solutions. *Journal of Geophysical Research*, 107. <https://doi.org/10.1029/2001jd000557>
- Kim, J. H., & Lee, H. (2010). What causes the springtime tropospheric ozone maximum of Northeast Asia? *Advances in Atmospheric Sciences*, 27, 543–551. <https://doi.org/10.1007/s00376-009-9098-z>
- Lachmy, O., & Harnik, N. (2014). The transition to a subtropical jet regime and its maintenance. *Journal of the Atmospheric Sciences*, 71, 1389–1409. <https://doi.org/10.1175/JAS-D-13-0125.1>
- Langford, A. O. (1999). Stratosphere-troposphere exchange at the subtropical jet: Contribution to the tropospheric ozone budget at midlatitudes. *Geophysical Research Letters*, 26, 2449–2452. <https://doi.org/10.1029/1999gl900556>
- Langford, A. O., Brioude, J., Cooper, O. R., Senff, C. J., Alvarez, R. J., Hardesty, R. M., et al. (2012). Stratospheric influence on surface ozone in the Los Angeles area during late spring and early summer of 2010. *Journal of Geophysical Research*, 117. <https://doi.org/10.1029/2011jd016766>
- Lee, S.-M., & Cheng, Y.-L. (2011). An examination of ENSO's effect on the monthly and seasonal climate of Hong Kong from a statistical perspective. *Acta Meteorologica Sinica*, 25, 34–50. <https://doi.org/10.1007/s13351-011-0003-1>
- LeGrand, S. L., Polashenski, C., Letcher, T. W., Creighton, G. A., Peckham, S. E., & Cetola, J. D. (2019). The AFWA dust emission scheme for the GOCART aerosol model in WRF-Chem v3.8.1. *Geoscientific Model Development*, 12, 131–166. <https://doi.org/10.5194/gmd-12-131-2019>
- Lin, M., Fiore, A. M., Horowitz, L. W., Cooper, O. R., Naik, V., Holloway, J., et al. (2012). Transport of Asian ozone pollution into surface air over the western United States in spring. *Journal of Geophysical Research*, 117, D00V07. <https://doi.org/10.1029/2011JD016961>
- Liu, G., Liu, J., Tarasick, D. W., Fioletov, V. E., Jin, J. J., Moeni, O., et al. (2013). A global tropospheric ozone climatology from trajectory-mapped ozone soundings. *Atmospheric Chemistry and Physics*, 13(21), 10659–10675. <https://doi.org/10.5194/acp-13-10659-2013>
- Liu, G., Tarasick, D. W., Fioletov, V. E., Sioris, C. E., & Rochon, Y. J. (2009). Ozone correlation lengths and measurement uncertainties from analysis of historical ozonesonde data in North America and Europe. *Journal of Geophysical Research*, 114, D04112. <https://doi.org/10.1029/2008JD010576>
- Ma, X., Huang, J., Zhao, T., Liu, C., Zhao, K., Xing, J., & Xiao, W. (2021). Rapid increase in summer surface ozone over the North China Plain during 2013–2019: A side effect of particulate matter reduction control? *Atmospheric Chemistry and Physics*, 21, 1–16. <https://doi.org/10.5194/acp-21-1-2021>
- Meloan, J., Siegmund, P. C., & Sigmund, M. (2001). A Lagrangian computation of stratosphere-troposphere exchange in a tropopause folding event in the subtropical southern hemisphere. *Tellus A: Dynamic Meteorology and Oceanography*, 53, 368–379. <https://doi.org/10.1034/j.1600-0870.2001.01175.x>
- Meul, S., Langematz, U., Kröger, P., Oberländer-Hayn, S., & Jöckel, P. (2018). Future changes in the stratosphere-to-troposphere ozone mass flux and the contribution from climate change and ozone recovery. *Atmospheric Chemistry and Physics*, 18(10), 7721–7738. <https://doi.org/10.5194/acp-18-7721-2018>
- Mills, G., Pleijel, H., Malley, C. S., Sinha, B., Cooper, O. R., Schultz, M. G., et al. (2018). Tropospheric ozone assessment report: Present-day tropospheric ozone distribution and trends relevant to vegetation. *Elementa: Science of the Anthropocene*, 6(1), 47. <https://doi.org/10.1525/elementa.302>
- Monks, P. S., Archibald, A. T., Colette, A., Cooper, O., Coyle, M., Derwent, R., et al. (2015). Tropospheric ozone and its precursors from the urban to the global scale from air quality to short-lived climate forcer. *Atmospheric Chemistry and Physics*, 15(15), 8889–8973. <https://doi.org/10.5194/acp-15-8889-2015>
- Nakamura, H. (1992). Midwinter suppression of baroclinic wave activity in the Pacific. *Journal of the Atmospheric Sciences*, 49, 1629–1642. [https://doi.org/10.1175/1520-0469\(1992\)049<1629:msbwa>2.0.co;2](https://doi.org/10.1175/1520-0469(1992)049<1629:msbwa>2.0.co;2)
- Ni, Z., Luo, K., Gao, X., Gao, Y., Fan, J. R., Fu, J. S., & Chen, C. H. (2019). Exploring the stratospheric source of ozone pollution over China during the 2016 Group of Twenty summit. *Atmospheric Pollution Research*, 10(4). <https://doi.org/10.1016/j.apr.2019.02.010>
- Oltmans, S. J., Johnson, B. J., Harris, J. M., Thompson, A. M., Liu, H. Y., Voemel, H., et al. (2004). Tropospheric ozone over the North Pacific from ozonesonde observations. *Journal of Geophysical Research*, 109, D15S01. <https://doi.org/10.1029/2003jd003466>
- Pendlebury, D., Gravel, S., Moran, M. D., & Lupu, A. (2018). Impact of chemical lateral boundary conditions in a regional air quality forecast model on surface ozone predictions during stratospheric intrusions. *Atmospheric Environment*, 174, 148–170. <https://doi.org/10.1016/j.atmosenv.2017.10.052>

- Rao, T. N., Arvelius, J., & Kirkwood, S. (2008). Climatology of tropopause folds over a European Arctic station (Esrange). *Journal of Geophysical Research*, *113*, D00B03. <https://doi.org/10.1029/2007JD009638>
- Rowlinson, M., Rap, A., Hamilton, D., Pope, R., Hantson, S., Arnold, S., et al. (2020). Tropospheric ozone radiative forcing uncertainty due to pre-industrial fire and biogenic emissions. *Atmospheric Chemistry and Physics*, *20*, 10937–10951. <https://doi.org/10.5194/acp-2019-1065>
- Schlemmer, L., Martius, O., Sprenger, M., Schwierz, C., & Twitchett, A. (2010). Disentangling the forcing mechanisms of a heavy precipitation event along the Alpine south side using potential vorticity inversion. *Monthly Weather Review*, *138*(6), 2336–2353. <https://doi.org/10.1175/2009mwr3202.1>
- Scott, R. K., & Cammas, J. P. (2002). Wave breaking and mixing at the subtropical tropopause. *Journal of the Atmospheric Sciences*, *59*(15), 2347–2361. [https://doi.org/10.1175/1520-0469\(2002\)059<2347:wbamat>2.0.co;2](https://doi.org/10.1175/1520-0469(2002)059<2347:wbamat>2.0.co;2)
- Sicard, P., Agathokleous, E., Araminiene, V., Carrari, E., Hoshika, Y., De Marco, A., & Paoletti, E. (2018). Should we see urban trees as effective solutions to reduce increasing ozone levels in cities? *Environmental Pollution*, *243*, 163–176. <https://doi.org/10.1016/j.envpol.2018.08.049>
- Sinclair, V. A., Belcher, S. E., & Gray, S. L. (2010). Synoptic controls on boundary-layer characteristics. *Boundary-Layer Meteorology*, *134*(3). <https://doi.org/10.1007/s10546-009-9455-6>
- Singh, H. B., Brune, W. H., Crawford, J. H., Jacob, D. J., & Russell, P. (2006). Overview of the summer 2004 Intercontinental Chemical Transport Experiment–North America (INTEX-A). *Journal of Geophysical Research*, *111*(D24). <https://doi.org/10.1029/2006jd007905>
- Sprenger, M., Croci Maspoli, M., & Wernli, H. (2003). Tropopause folds and cross-tropopause exchange: A global investigation based upon ECMWF analyses for the time period March 2000 to February 2001. *Journal of Geophysical Research*, *108*(D12), 8518. <https://doi.org/10.1029/2002JD002587>
- Stockwell, W. R., Middleton, P., Chang, J. S., & Tang, X. (1990). The second generation regional acid deposition model chemical mechanism for regional air quality modeling. *Journal of Geophysical Research*, *95*, 16343–16367. <https://doi.org/10.1029/jd095id10p16343>
- Tai, A. P. K., Martin, M. V., & Heald, C. L. (2014). Threat to future global food security from climate change and ozone air pollution. *Nature Climate Change*, *4*, 817–821. <https://doi.org/10.1038/nclimate2317>
- Tang, Q., Prather, M. J., & Hsu, J. (2011). Stratosphere-troposphere exchange ozone flux related to deep convection. *Geophysical Research Letters*, *38*. <https://doi.org/10.1029/2010GL046039>
- Tang, Y., Carmichael, G. R., Woo, J.-H., Thongboonchoo, N., Kurata, G., Uno, I., et al. (2003). Influences of biomass burning during the Transport and Chemical Evolution Over the Pacific (TRACE-P) experiment identified by the regional chemical transport model. *Journal of Geophysical Research*, *108*(D21), 8824. <https://doi.org/10.1029/2002JD003110>
- Van Haver, P., De Muer, D., Beekmann, M., & Mancier, C. (1996). Climatology of tropopause folds at midlatitudes. *Geophysical Research Letters*, *23*, 1033–1036. <https://doi.org/10.1029/96gl00956>
- Verstraeten, W. W., Neu, J. L., Williams, J. E., Bowman, K. W., Worden, J. R., & Boersma, K. F. (2015). Rapid increases in tropospheric ozone production and export from China. *Nature Geoscience*, *8*(9), 690–695. <https://doi.org/10.1038/ngeo2493>
- Wang, T., Wei, X. L., Ding, A. J., Poon, C. N., Lam, K. S., Li, Y. S., et al. (2009). Increasing surface ozone concentrations in the background atmosphere of Southern China, 1994–2007. *Atmospheric Chemistry and Physics*, *9*, 6216–6226. <https://doi.org/10.5194/acp-9-6217-2009>
- Westervelt, D. M., Ma, C. T., He, M. Z., Fiore, A. M., Kinney, P. L., Kioumourtzoglou, M., et al. (2019). Mid-21st century ozone air quality and health burden in China under emissions scenarios and climate change. *Environmental Research Letters*, *14*, 74030. <https://doi.org/10.1088/1748-9326/ab260b>
- Zahn, A., Brenninkmeijer, C. A. M., Asman, W. A. H., Crutzen, P. J., Heinrich, G., Fischer, H., et al. (2002). Budgets of O₃ and CO in the upper troposphere: CARIBIC passenger aircraft results 1997–2001. *Journal of Geophysical Research*, *107*(D17), 4337. <https://doi.org/10.1029/2001JD001529>
- Zhang, Y., Cooper, O., Gaudel, A., Thompson, A. M., Nédélec, P., Ogino, S., & West, J. J. (2016). Tropospheric ozone change from 1980 to 2010 dominated by equatorward redistribution of emissions. *Nature Geoscience*, *9*, 875–879. <https://doi.org/10.1038/ngeo2827>
- Zhang, Y., Mao, H., Ding, A., Zhou, D., & Fu, C. (2013). Impact of synoptic weather patterns on spatio-temporal variation in surface O₃ levels in Hong Kong during 1999–2011. *Atmospheric Environment*, *73*, 41–50. <https://doi.org/10.1016/j.atmosenv.2013.02.047>
- Zhao, K., Bao, Y., Huang, J., Wu, Y., Moshary, F., Arend, M., et al. (2019). A high-resolution modeling study of a heat wave-driven ozone exceedance event in New York City and surrounding regions. *Atmospheric Environment*, *199*, 368–379. <https://doi.org/10.1016/j.atmosenv.2018.10.059>
- Zhao, K., Hu, C., Yuan, Z., Xu, D., Zhang, S., Luo, H., et al. (2021). A modeling study of the impact of stratospheric intrusion on ozone enhancement in the lower troposphere over the Hong Kong regions, China. *Atmospheric Research*, *247*, 105158. <https://doi.org/10.1016/j.atmosres.2020.105158>